Supporting Information

Water oxidation by amorphous cobalt-based oxides: *in-situ* tracking of redox transitions and mode of catalysis

Marcel Risch,[1,2] *Franziska Ringleb,*[1,3] *Mike Kohlhoff,*[1,4]
Peter Bogdanoff,[5] *Petko Chernev,*[1] *Ivelina Zaharieva,*[1] *Holger Dau*[1*]

[1] Freie Universität Berlin, FB Physik, Arnimallee 14, 14195 Berlin, Germany;

[2] present address: Research Laboratory of Electronics, Massachusetts Institute of Technology, 77 Massachusetts Ave, Cambridge, MA 02139, USA;

[3] present address: Fritz-Haber-Institut der Max-Planck-Gesellschaft, Faradayweg 4-6, 14195 Berlin, Germany;

[4] present address: Department of Chemistry, University of Oxford, Chemistry Research Laboratory, Oxford OX1 3TA, United Kingdom

[5] Helmholtz-Zentrum Berlin, Institute of Solar Fuels and Energy Storage Materials, Hahn-Meitner-Platz 1, 14109 Berlin, Germany.

EXPERIMENTAL SECTION

Materials

All solutions were prepared from purified, deionized water (Millipore milliQ water, >18 MΩ·cm). Solutions of inorganic potassium phosphate, KP_i, were prepared as a mixture of ~ 40% KH_2PO_4 and ~ 60% K_2HPO_4 at a total P_i concentration of 0.1 M; we verified that the pH of the resulting electrolyte was 7.0 (or verified adjustment to 8.0 or 9.0 in specific in-situ experiments). The source of the electrodeposited Co^{II} ions was cobalt nitrate solution of 0.5 mM concentration (in 0.1 M phosphate buffer). Electrodeposition and all electrochemical experiments were performed in 0.1 M phosphate buffer.

Material	Formula	Purity	Supplier	Head office
Potassium phosphate	KH_2PO_4	99.5 %	AppliChem GmbH	Darmstadt, GER
Potassium phosphate, dibasic	K_2HPO_4	99.5 %	AppliChem GmbH	Darmstadt, GER
Cobalt nitrate	$Co^{II}(OH_2)_6(NO_3)_2$	99.9 %	Sigma Aldrich Chemie GmbH	Munich, GER
Hydrochloric acid	HCl	30 %	Carl Roth GmbH	Karlsruhe, GER
ITO on glass	n/a	8-12 Ω/sq	Sigma Aldrich GmbH	Munich, GER
ITO on PET	n/a	45 Ω/sq	Sigma Aldrich GmbH	Munich, GER
Pt electrode, 100 mesh	n/a	99.9%	Sigma Aldrich GmbH	Munich, GER
Glassy carbon SIGRADUR K	n/a	n/a	HTW Hochtemperatur-Werkstoffe GmbH	Thierhaupten, GER
Co foil, 10 µm	Co	99.9 %	Goodfellow GmbH	Bad Nauheim, GER

Electrochemistry

All potentials are given relative to the normal hydrogen electrode (NHE). A mercury sulfate reference electrode (650 mV vs. NHE) and a either Micro-Autolab Type III potentiostat (Metrohm Autolab B.V., Utrecht) or SP-200 potentiostat (Bio-Logic, Claix, France) were used for electrochemical characterization. Unless otherwise noted, the potential axis (V) was corrected for the internal resistance of the working electrode and the electrolyte solution by the following equation:

$$V_{corrected} = V_{measured} - iR, \quad \text{(S1)}$$

where *i* is the current and *R* the resistance. The value of *R* was estimated in an auxiliary experiment using potentiostatic electrochemical impedance spectroscopy (PEIS) performed on an SP-200 potentiostat (Bio-Logic, Claix, France).

In the experiments of Fig. 8 (of the main text), the potentiostat (SP-200, Bio-Logic) switched within a few microseconds from application of a constant voltage (potentiostatic mode) and simultaneous current detection to an open-circuit mode. In the open-circuit mode (electrometer mode), the high input impedance of the potentiostat (>10^{12} Ohms) prevented any current flow and the electrode voltage (open-circuit voltage) was recorded with a spacing between data points of 200 µs.

Elemental analysis

The total X-ray reflection fluorescence analysis (TXRF) was performed on a Bruker AXS PICOFOX using cobalt catalyst (CoCat) films dissolved in HCl (30 %). Gallium solution (Fluka TraceCert) of known concentration was added as a standard for quantitative analysis.

Sample preparation and cell for *in-situ* XAS

CoCat-coated electrodes were prepared in a separate electrochemical setup before start of the *in-situ* XAS measurements. The electrochemical setup for deposition was a three-electrode setup driven by a Micro-Autolab Type III potentiostat (Metrohm Autolab B.V., Utrecht). A 25 x 25 mm² platinum grid served as the counter electrode and the reference was a mercury sulfate electrode (+650 mV vs. NHE; Schott GmbH). CoCat films were deposited on 125 µm thick polyethylene terephthalate (PET) slides coated with indium tin oxide (ITO). An area of 2 cm × 2 cm was exposed to the electrolyte, which contained 0.5 mM Co^{2+} ions and 0.1 M KP_i (pH 7). The CoCat films were deposited at 1.05 V until a charge of 5 mC·cm^{-2} had passed, which corresponds to deposition of about 50 nmol of Co ions by one-electron oxidation of Co^{II} to Co^{III}. The potential was not corrected for the *iR* drop because (at 1.05 V) the low currents render the influence of the *iR* drop negligible. The CoCat films were stored for maximally 24 h at room conditions before measurement. We did not detect any differences in the XAS measurements between freshly prepared films and those that we had stored for a several hours.

The electrochemical cell for XAS measurements was driven by an SP-200 potentiostat (Bio-Logic, Claix, France). The counter electrode was a 25 x 25 mm² platinum grid (100 mesh, 99.9 %, Sigma Aldrich GmbH) and a saturated mercury sulfate reference electrode (+650 mV *vs.* NHE; Schott GmbH) were used. The electrolyte was not stirred during the X-ray measurements to avoid an increase in noise of the fluorescence signal.

XAS sample preparation – freeze-quench method

The freeze-quench XAS approach involved the following five stages as detailed in the main text: (1) CoCat formation in the XAS sample holder. (2) interrogation of the redox-behavior of the CoCat film in Co-free KPi. (3) Potentiostatic equilibration for two min at the desired potential. (4) Immersion in liquid nitrogen. (5) Synchrotron measurements.

The working electrodes were 100 µm thin plates of glassy carbon. Sample cells were constructed by gluing these glassy carbon electrodes to a 2 mm thick PVC sample holder, into which a 13 mm x 13 mm window had been cut. A loop of platinum wire measuring 4.5 cm with diameter 0.3 mm served as counter electrode. These sample cells exhibited a resistance of 10 Ω when filled with 100 mM $KP_{i,}$ buffer, as determined by impedance spectroscopy.

In cyclic voltammetry (CV) control experiments, the current density of the previously cleaned working electrodes was lower than 5 µA·cm^{-2} (at 1.35 V vs. NHE, pH 7), whereas the current density after deposition was approximately 1 mA·cm^{-2} at the same potential. The cobalt catalyst film (CoCat) was deposited at 1.35 V for 10 min in KP_i electrolyte with 0.5 mM Co^{2+}. The resulting films contained about 50 nmol·cm^{-2} of cobalt (as determined by TXRF analysis). The sample holders were flushed several times with cobalt-free KP_i before the electrochemical experiments were initiated in cobalt-free KP_i. Quasi steady-state conditions were approximated by waiting for 2 min before the samples were frozen. This duration was sufficiently long to develop a nearly stable steady-state current. At 1.49 V, the current response was still decaying. The duration of two min was chosen as a trade-off between achieving quasi steady-state currents and preventing film dissolution.

After selection of the desired potential at the working electrode, the potential difference between the working and counter electrode was measured. Subsequently, the reference electrode was removed from the setup and a stabilized DC power supply was used to apply the previously determined potential difference as a voltage between working and counter electrode. After two further minutes had passed, liquid nitrogen was used to quickly freeze the sample cell while the potential was applied. This means that the voltage between working and counter electrode was removed only after having frozen the CoCat film. Then the sample cells were stored in liquid nitrogen (for maximally two weeks) before they were measured by X-ray absorption spectroscopy at 20 K.

EXAFS simulations

The spectra were normalized and EXAFS oscillations were extracted as described in ref. 35. For conversion of the energy axis to a *k*-vector axis, an E_0 of 7710 eV was used; interpolation yielded equidistant points on a *k*-vector axis (Δk = 0.075 Å^{-1}) All simulations were performed using the in-house software packages 'SimX' (Dittmer 1999) and 'SimX lite' (written by Dr. Petko Chernev). An amplitude reduction factor S_0^2 of 0.7 and an energy correction shift (ΔE_0) of +1.5 eV were used in the simulations.

We will briefly describe the 'EXAFS equation'. An EXAFS spectrum χ(k) is given by the sum of the contributions of *n* 'atomic shells'. A 'shell' is a group of elements with identical atomic number and similar distances from the X-ray absorbing atom, *e.g.,* six oxygen atoms surrounding the absorbing cobalt ion in the CoCat. The EXAFS equation is mathematically defined as follows:

$$\chi(k) = S_0^2 \sum_i^n A_i \cdot N_i \cdot \exp\left(-2\sigma_i^2 \cdot k^2\right) \cdot \frac{\sin\left(2k \cdot R_i + \phi_i\right)}{kR_i^2} \quad , \qquad \text{(S2)}$$

where S_0^2 is the amplitude reduction factor, $A(R_i,k)_i$ is an amplitude-modifying factor and $\phi(k)_i$ is the phase correction (both were obtained herein from *ab-initio* FEFF calculations),[2,3] N_i is the

number of neighbors in the i^{th} atomic shell, σ_i is the Debye-Waller parameter of the i^{th} atomic shell, and R_i is the distance between the absorber and the atoms in the i^{th} atomic shell. It is well established that A_i does not depend significantly on the number of ligands or the oxidation state (phase transferability[4]).

For the analysis of the freeze-quench data, the phase functions were calculated using FEFF 8.4.[2,5] Atomic coordinates of the FEFF input files were generated on basis of the model structure shown in ref. 6. Only single scattering paths were employed in the simulations.

For the analysis of the *in-situ* measurements, the phase functions were obtained by *ab-initio* simulations using FEFF 9.05.[3,5] For the simulation at the cobalt *K*-edge, the coordinates were taken from a CoO_2 layer fragment of the $LiCoO_2$ structure with 10 cobalt atoms and 32 oxygen atoms, which is shown in ref. 7. Only single scattering paths were employed in the simulations. The simulation results with the new phase functions for cobalt obtained by using FEFF 9.05 did not deviate significantly from those used for simulation obtained by using FEFF 8.4. However, the energy shift of E_0 (relative to the value used for extraction of the experimental EXAFS data) was increased to 3.5 eV (as found by EXAFS simulations of the experimental data).

Estimation of the formal oxidation state using XANES data

In the freeze-quench experiments, a cobalt metal foil was used as an energy reference; its spectrum was measured simultaneously during collection of the fluorescence data on the CoCat sample. Analysis of this references spectrum using a highly standardized protocol involving derivative calculation (first inflection point at 7709 eV) and curve-fitting typically provides an energy calibration with an energy uncertainty below 0.1 eV. We find that the rising part of the pre-edge of cobalt oxides is observable at the same X-ray energy (within 0.1 eV), irrespective of the of the cobalt oxidation state. In the in-situ experiments, precise energy calibration thus could be achieved by aligning the rising part of the pre-edge peaks to the pre-edge rise of ex-situ spectra determined before (data form refs. 25, 40 of the main manuscript).

For the conversion of the (integral) edge position to the formal oxidation state, we used the known oxidation states of the following compounds to obtain a calibration curve: $(Co^{II}OH_2)_6(NO_3)_2$ solution, $(Co^{II}OH_2)_6(NO_3)_2$ powder, $Co^{II}{}_3(PO_4)_2$ powder, $Co^{II,III}{}_3O_4$ powder (formal oxidation state +2.67), $Co^{III}OOH$ powder (kindly provided by Dr. Anna Fischer, TU Berlin), $LiCo^{III}O_2$ powder.

Numerical values for an edge-position energy were obtained by calculation of the integral of the edge region calculated between μ = 0.15 and 1.0 (integral method, see ref. 8). The result of linear regression using the corresponding data analysis tools of Origin 8.1 ('Fit linear') was a slope of (2.30 ± 0.04) eV per oxidation-state unit. The energy offset (*i.e.* axis intercept of the regression line) was 7713.94 eV. The coefficient of determination R^2 was 99.83 % (R^2 = 1- [residual sum of squares]/[total sum of squares]). This figure supports that the integral edge positions increase linearly with the oxidation state, to a good approximation, as reported also for manganese oxides.[8] The errors of the oxidation state (v) were calculated by Gaussian error progression using the following formula

$$\Delta v = \sqrt{\left(\frac{\Delta Y}{a}\right)^2 + \left(\frac{-\Delta b}{a}\right)^2 + \left(\frac{[Y - b] \cdot \Delta a}{a^2}\right)^2} \quad \text{(S3)}$$

,

where Y is the edge position, a is the slope of the calibration curve and b is the energy offset. Δ denotes the standard error (68 % confidence interval). The error range of the oxidation equivalent was obtained by squaring the standard errors obtained for 0.80 V and 1.49 V and taking the root of the sum (Gaussian error propagation as in Eq. S3).

The relative populations of Co^{II}, Co^{III} and Co^{IV} were calculated using:

$$z = 2[Co^{II}] + 3[Co^{III}] + 4[Co^{IV}], \quad \text{(S4a)}$$

where z denotes the mean oxidation state from XAS analysis and sum of the relative cobalt concentrations equals unity ($[Co^{II}] + [Co^{III}] + [Co^{IV}] = 1$).

Assuming that $[Co^{IV}]$ is negligibly small at low potentials, we now obtain:

$$[Co^{III}] = z - 2; \; [Co^{II}] = 1 - [Co^{III}] \quad \text{(S4b)}$$

Assuming that $[Co^{II}]$ is negligibly small at high potentials, we obtain:

$$[Co^{IV}] = z - 3; \; [Co^{III}] = 1 - [Co^{IV}] \quad \text{(S4c)}$$

Area of gold surface in DEMS experiments

The electrochemical characteristics of the gold surface were measured prior to CoCat deposition (see Fig. S6). We estimated the enlargement of the surface area of a porous gold electrode by integration of the oxygen reduction wave. A value of 1.82 $mC \cdot cm^{-2}$ was obtained. The literature value is 0.48 $mC \cdot cm^2$ for a gold electrode in the absence of surface enlargement.[9] Therefore, we estimate an enlargement of the surface of the gold electrode by a factor of 3.8.

UV-Vis spectroscopy

In the UV-VIS experiment, electrolyte, ITO working electrode, Pt counter electrode, and a mercury-sulfate reference electrode were positioned inside of an optical UV-Vis cuvette (20 x 20 x 50 mm, dye-laser quartz cuvette, Hellma GmbH, Müllheim). Optical absorption spectra were recorded on a Cary 50 UV-Vis spectrophotometer (Varian GmbH, Waldbronn). The films were equilibrated at the desired potentials for 90 s before recording a spectrum. All spectra were measured with the cobalt-free KP_i electrolyte present. (Before measurement, the films for UV-Vis experiments were deposited on an ITO electrode in KP_i (0.1 M; pH 7). The concentration of Co^{II} ions was 0.5 mM; a potential of 1.33 V (*iR* corrected value) was applied for 10 min.)

Calculation of UV-Vis extinction coefficient of the CoCat film

The molar extinction coefficient, ε, of an ionic or molecular species in a solution is defined as:

$$\varepsilon(\lambda) = - \log_{10}(I/I_0) / (d\, c), \quad \text{(S5)}$$

where I and I_0 are the light intensities before and after the sample, respectively, d is the optical path length (in cm) and c the molar concentration of the ionic species (in mol/L). The value of $\log_{10}(I/I_0)$ corresponds to the decadic absorbance, which is denoted by A throughout this manuscript. The extinction coefficient is most commonly expressed in non-SI units of $L \cdot mol^{-1} \cdot cm^{-1}$ (*e.g.,* in ref. [10]). Based on Eq. S5, we obtain an equation for the extinction coefficient of a CoCat film deposited on a transparent and planar electrode (for an angle of 90° between electrode surface and incident light beam):

$$\varepsilon(\lambda) = A / (n_{Co}\ 10^3\ cm^3\ L^{-1}), \qquad \text{(S6)}$$

with n_{Co} being the molar density of Co ions per cm^2 (n_{Co} in mol/cm^2). For example, we calculate for a molar density of 50 nmol of Co ions per cm^2 of electrode surface and decadic absorbance of 0.1, a value of the molar extinction coefficient of 2000 mol cm L^{-1} using Eq. S6. We note that the value of $\varepsilon(\lambda)$ depends on A and $n_{Co,}$ but does not depend on the film thickness.

Calculation of the catalytic current from UV-Vis absorption changes

The estimation of the catalytic currents (Fig. 8 of the main text) was obtained by calculation of the first derivative of absorption changes detected at 600 nm, yielding d*A600*/d*t*. The current densities were obtained using the herein established correlation between the optical absorption, the oxidation state from XAS analysis and the oxidative charges (Fig. 3 of the main text). The catalytic current density (j_{cat}) was calculated as:

$$j_{cat} = \frac{\mathrm{d}A600}{\mathrm{d}t} \cdot \frac{\mathrm{d}v}{\mathrm{d}A600} \cdot Q_{dep} \qquad \text{(S7)}$$

,

where Q_{dep} is the total charge during cobalt deposition, d*A600*/d*t* is the time-derivative of the absorbance at 600 nm (obtained from the data shown in Fig. 4 of the main text), d*v*/d*A* is the derivate of the oxidation states, *v*, calculated from XAS edge positions with respect to the absorbance, *A*. The value of d*v*/d*A600* was obtained from the data shown in Fig. 3 (of the main text).

Analytical solution of the modified Nernst equation

The classical Nernst equation was extended as discussed in the RESULTS section (of the main article) to describe the relation between the mean cobalt oxidation state (Y_i) and the electric potential of the electrode. Using the symbols introduced in the RESULTS section, combination of Eq. 2 and Eq. 3 and straightforward mathematical rearrangements results in:

$$Y_i(V) = \frac{Y_{max,i} \cdot \exp\{(eV - eE_{mi})/(k_B T + E_{0i}')\} + Y_{min,i}}{\exp\{(eV - eE_{mi})/(k_B T + E_{0i}')\} + 1} \qquad \text{(S8)}$$

,

In the CoCat, we encountered two well-separated redox transitions, namely the $Co^{II \rightarrow III}$ transition (E_{m1} of about 1.01 V) and the $Co^{III \rightarrow IV}$ transition (E_{m2} of about 1.22 V) spaced by more than 200 mV. Since the spacing between these redox transitions is relatively high, we assume that

Eq. S8 can be applied separately to the two individual redox transitions (to a good approximation) and we calculate the relation between the mean cobalt oxidation state and the electrode potential according to:

$$Y(V) = Y_1(V) + Y_2(V), \quad \text{(S9)}$$

with $Y_1(V)$ and $Y_2(V)$ calculated according to Eq. S8 (for i = 1 and i = 2, respectively). The parameters for the simulations shown in Figs. 2 and 6 (of the main text) can be found in Table S1.

Supporting Figures and Tables

Table S1. Parameters used in the simulations of Fig. 2 and 6 in the main text. For all simulations, $Y_{min,1} = 2.6$, $Y_{max,1} = Y_{min,2} = 3$, $Y_{max,2} = 3.25$, and $k_BT = 0.026$ eV (T = 300 K).

Figure	**pH**	$E_{01}' = E_{02}'$	E_{m1}	E_{m2}
2	9	*0.03*	0.85±0.02	0.99±0.03
2	8	*0.03*	0.92±0.01	1.10± 0.02
2, 6	7	*0.03*	1.03±0.04	1.25±0.06
6	7	*0.00*	1.03±0.03	1.26±0.04
6	7	*0.10*	1.12*	1.25*

Italicized parameters were fixed.
*We note that in this simulation the error was unreasonably high such that the determined midpoint potentials are not meaningful.

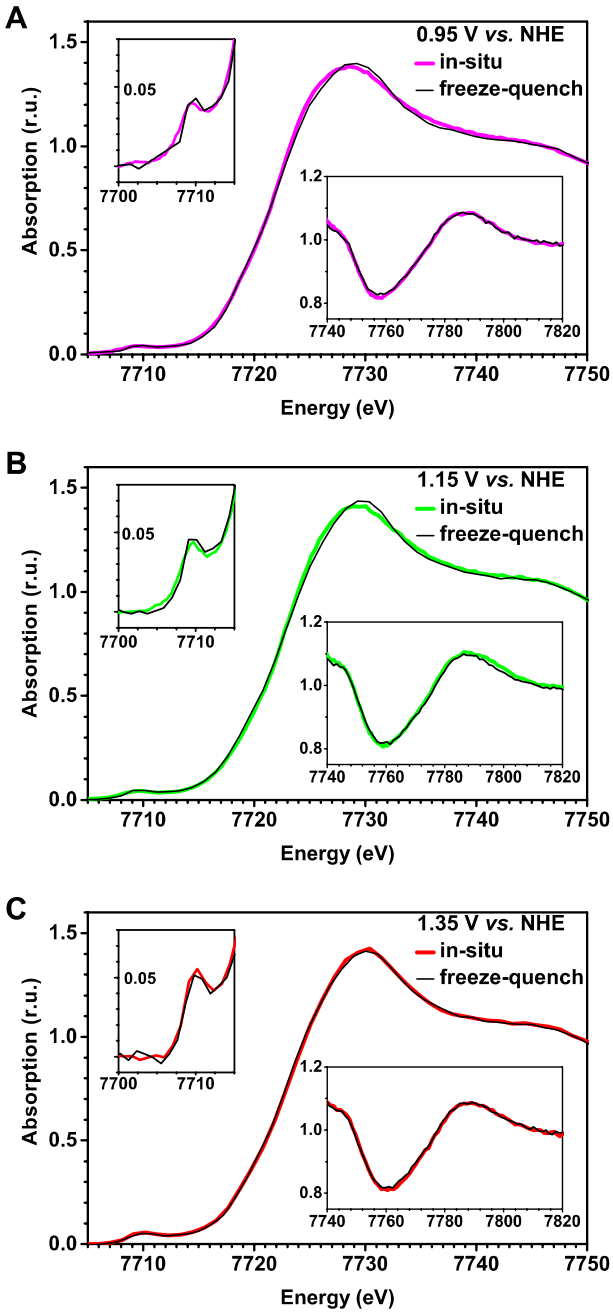

Figure S1. Comparison between X-ray absorption spectra of the CoCat obtained by the freeze-quench method (thin black line) and the *in-situ* method (colored thick lines) for (A) 0.95 V, (B) 1.05 V and (C) 1.35 V vs. NHE. The XAS measurements of the freeze-quench data were performed at 20 K, whereas in the *in-situ* experiments XAS data was collected at room temperature (300 K). The spectra match well, except for a broadening of the principal edge maximum (the 'white line') at lower potentials, presumably due to increased dynamic disorder in the coordination sphere at room temperature. Potentials were not corrected for the *iR* drop ($iR \leq 30$ mV). The left insets magnify the region of the pre-edge, while the right insets magnify the first oscillations of the EXAFS region.

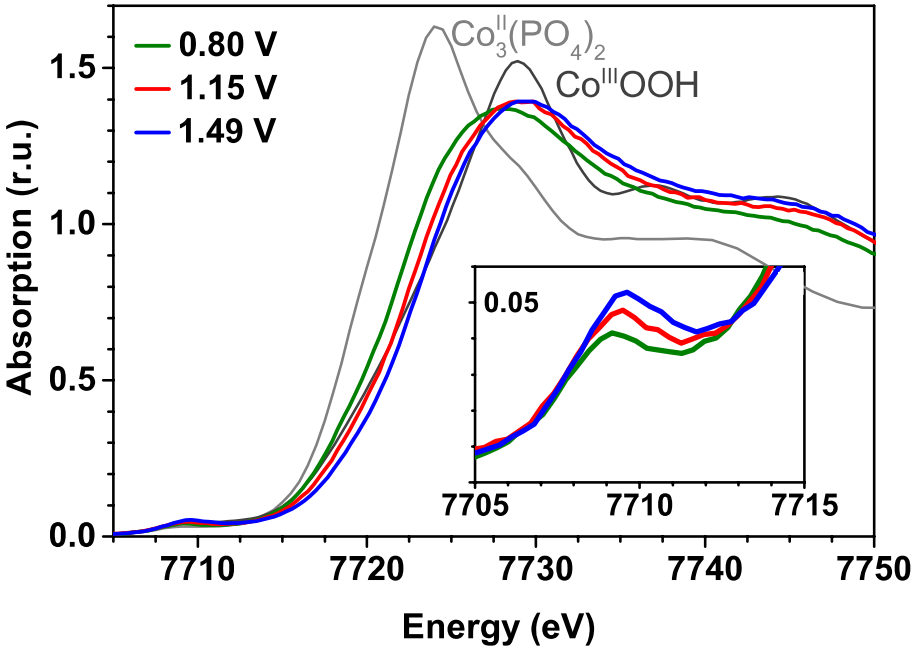

Figure S2. Shift in cobalt *K*-edge position of X-ray absorption spectra measured at 20 K using the freeze-quench method (standard CoCat samples, pH 7, indicated anode voltages *vs.* NHE) and reference spectra of $Co^{II}_3(PO_4)_2$, $Co^{III}OOH$. The inset magnifies the pre-edge region. The height and area of the pre-edge feature were found to increase for increasingly positive voltages. This is consistent with cobalt oxidation (explainable by increased *p-d* mixing of metal orbitals due to shortening of metal-oxygen distances upon oxidation[8,11]). The pre-edge height is also sensitive to the degree of symmetry around the metal center; highly asymmetric arrangements of ligands increase the pre-edge intensity.[12] Such a loss of symmetry could result from μ–O formation, which possibly relates to deprotonation of μ–OH bridges at higher potentials. The presence of μ–OH bridges in the all-Co^{III} oxidation state of the CoCat was recently supported by a combination of *ab-initio* molecular dynamics simulations (AIMD) and XAS.[13] The limited extent of increase in the pre-edge intensity suggests that, if present at all, Co^{IV}=O formation would relate to an exceedingly small minority fraction of cobalt ions only.

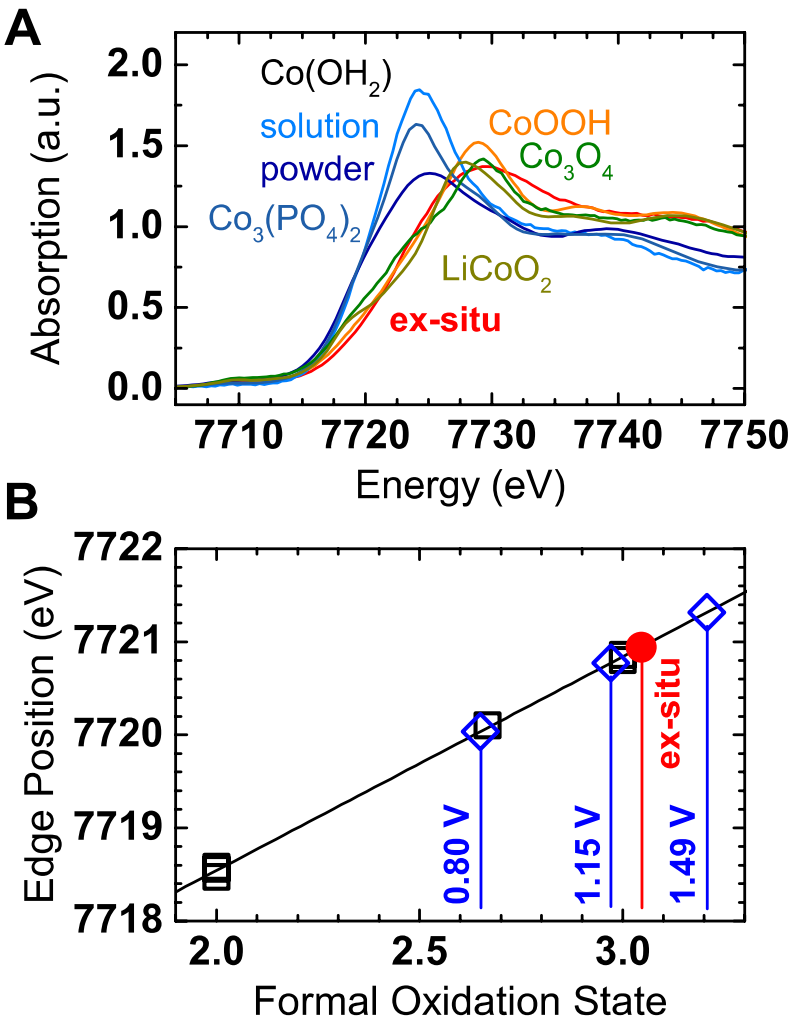

Figure S3. (A) Co *K*-edge XANES of $(Co^{II}OH_2)_6(NO_3)_2$ solution, $(Co^{II}OH_2)_6(NO_3)_2$ powder, $Co^{II}_3(PO_4)_2$ powder, $Co^{II, III}_3O_4$ powder, $Co^{III}OOH$ powder, $LiCo^{III}O_2$ powder (in order of ascending edge position) compared to a CoCat film measured *ex-situ*. (B) Empirical relation between the position of the cobalt *K*-edge as calculated by the integral method[8] with boundaries of μ = 0.15 to 1.0 (black line) and assignment of oxidation states to selected measurements. Black square symbols indicate the Co oxides in panel A. The blue diamonds represent selected measurements of the cobalt catalyst (CoCat, freeze-quench method at pH 7; spectra in Fig. S2). The red circle shows the edge position and oxidation state of a CoCat rinsed with distilled water after working as a water-oxidation catalysts at about 1.3 V (*vs.* NHE), rapidly dried, and frozen within two min.[6,14]

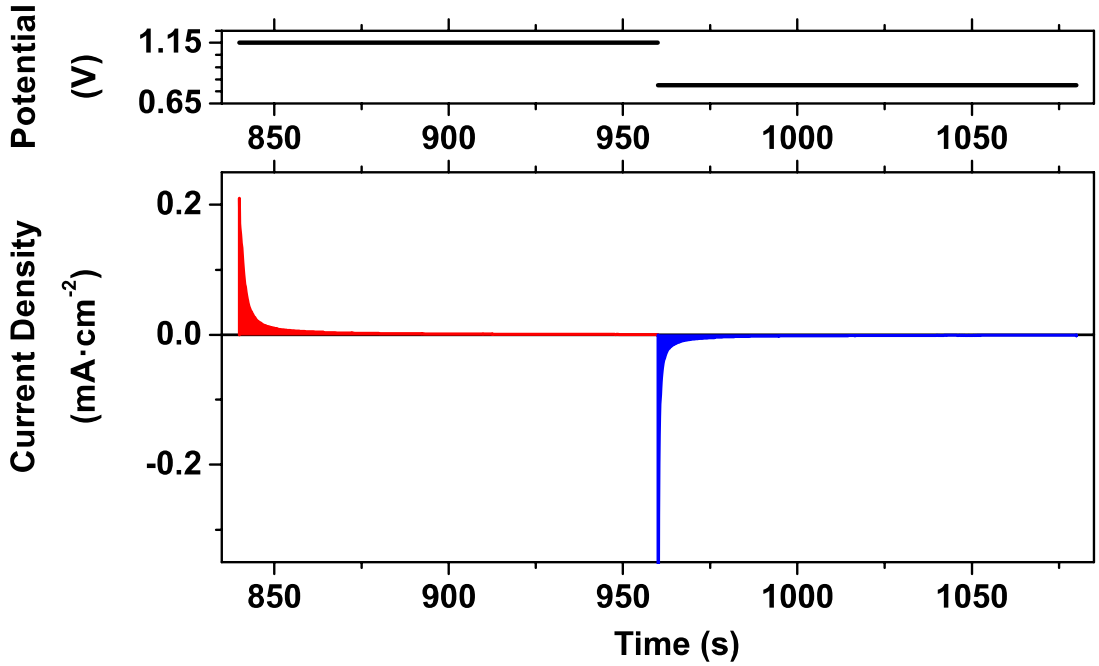

Figure S4. Graphical representation of the protocol used to estimate the amount of oxidative charging by coulometry (relates to respective data points in Fig. 3 of the main text). In this example, the CoCat film is held at 1.15 V for 2 min and subsequently exposed to 0.8 V, for reduction. A minor offset current was subtracted from the reduction current. Integration of the current over a time period of 60 s after the transition to 0.8 V yields the number of oxidation equivalents (blue area).

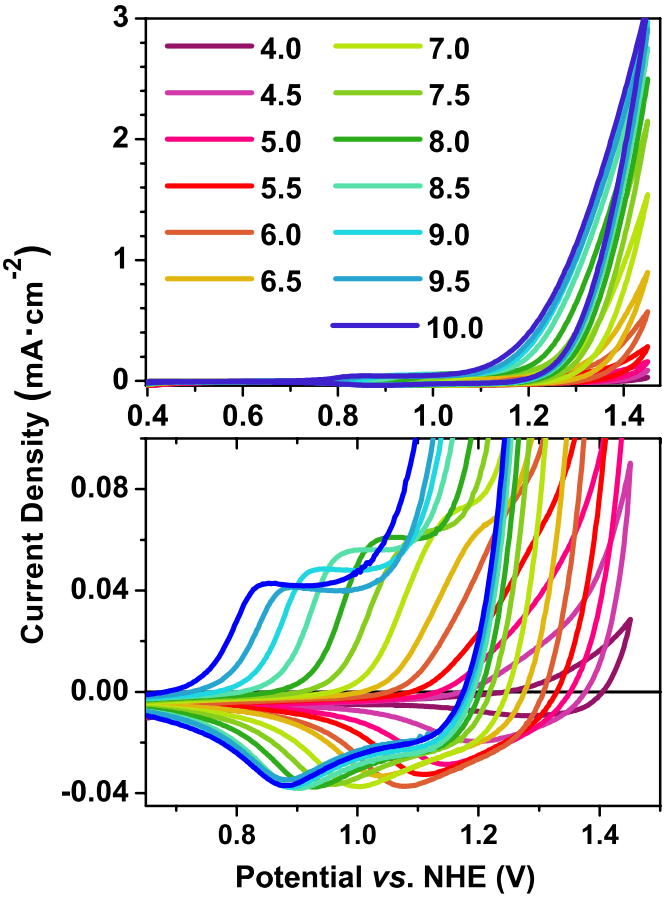

Figure S5. Cyclic voltammetry (CV) of the cobalt catalyst (CoCat) in 0.1 M KP_i solutions ranging in pH from 4 to 10. The top panel shows an increase of the catalytic current with pH. The shift of the pre-wave with pH is illustrated in the enlargement on the bottom. The scan rate was 20 $mV \cdot s^{-1}$. The potential axes were not corrected for the *iR* drop.

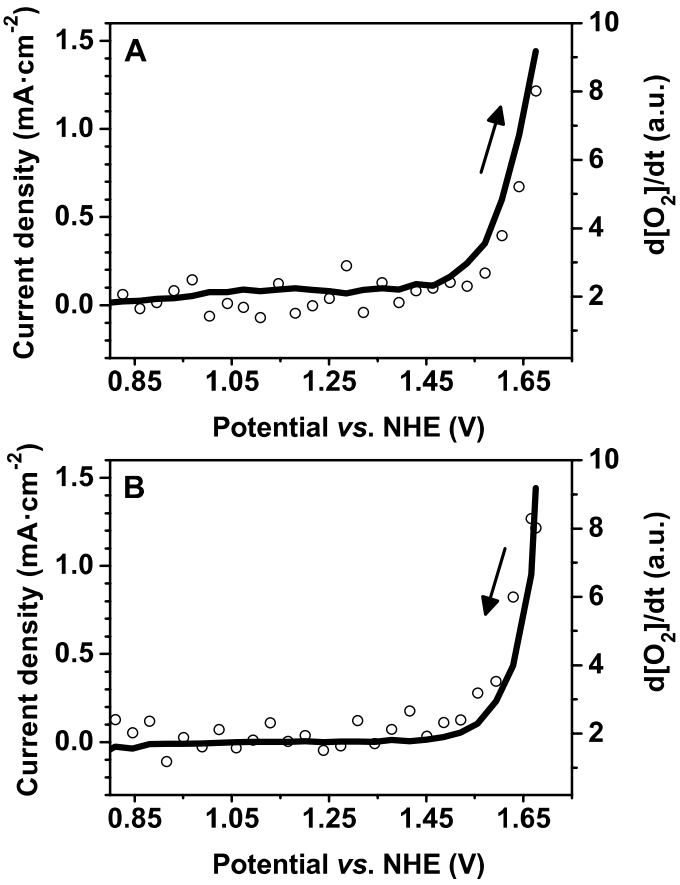

Figure S6. Electrochemical current (solid line) and oxygen evolution rate from DEMS (circles) of a bare gold electrode detected during a cyclic voltammogram (20 mV/s) for (A) increasing potential and (B) decreasing electrode potential. Arrows indicate the scan direction. The shift between current and DEMS signal suggests a response time for O_2 detection by the DEMS setup of about 1 s.

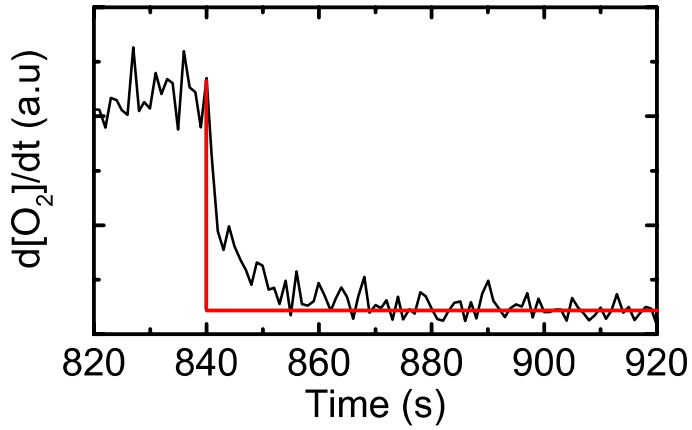

Figure S7. Oxygen-evolution rate of a cobalt-based catalyst film (CoCat) detected by membrane-inlet mass spectroscopy (DEMS) after switching from 1.38 V vs. NHE (pH 7) to open-circuit conditions (at 840 s). The vertical red line indicates the switching to open-circuit conditions (OC); the horizontal red line indicates the baseline (zero oxygen evolution). The time range of the 'delayed' O_2-formation after switching to OC is in agreement with the delay between current and O_2-formation in the cyclic voltammogram of Figure 7 and is compatible with the fast decrease in the slope of the A_{600} signal in Figure 8. This data provides direct support for water oxidation without any applied electrode voltage using solely previously accumulated oxidizing equivalents.

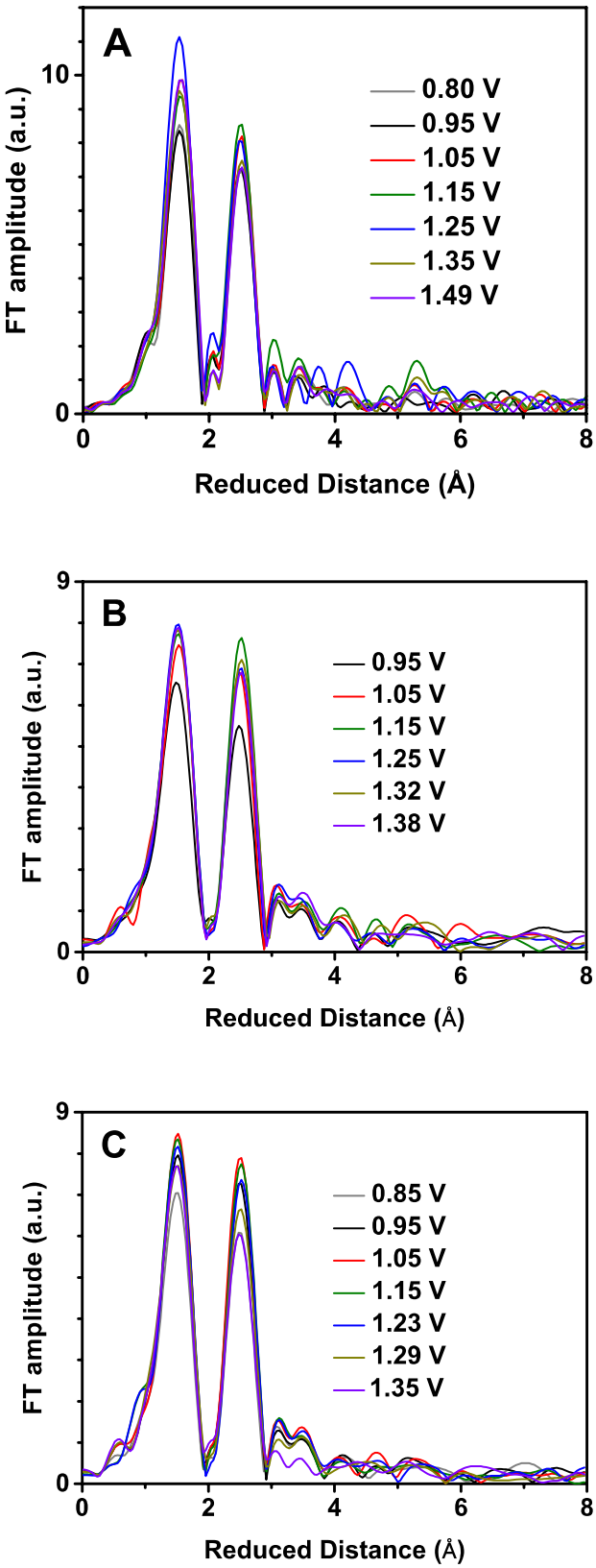

Figure S8. Fourier transforms of the EXAFS of (A) freeze-quench measurements at pH 7, (B) *in-situ* measurements at pH 7 and (C) *in-situ* measurements at pH 9. The reduced distances on the x-axis were obtained by Fourier transforming the unfiltered *k*-space data between 3 $Å^{-1}$ and 11.5 $Å^{-1}$; the internuclear distances determined by EXAFS simulations are by 0.3 Å to 0.4 Å longer than the indicated distances.

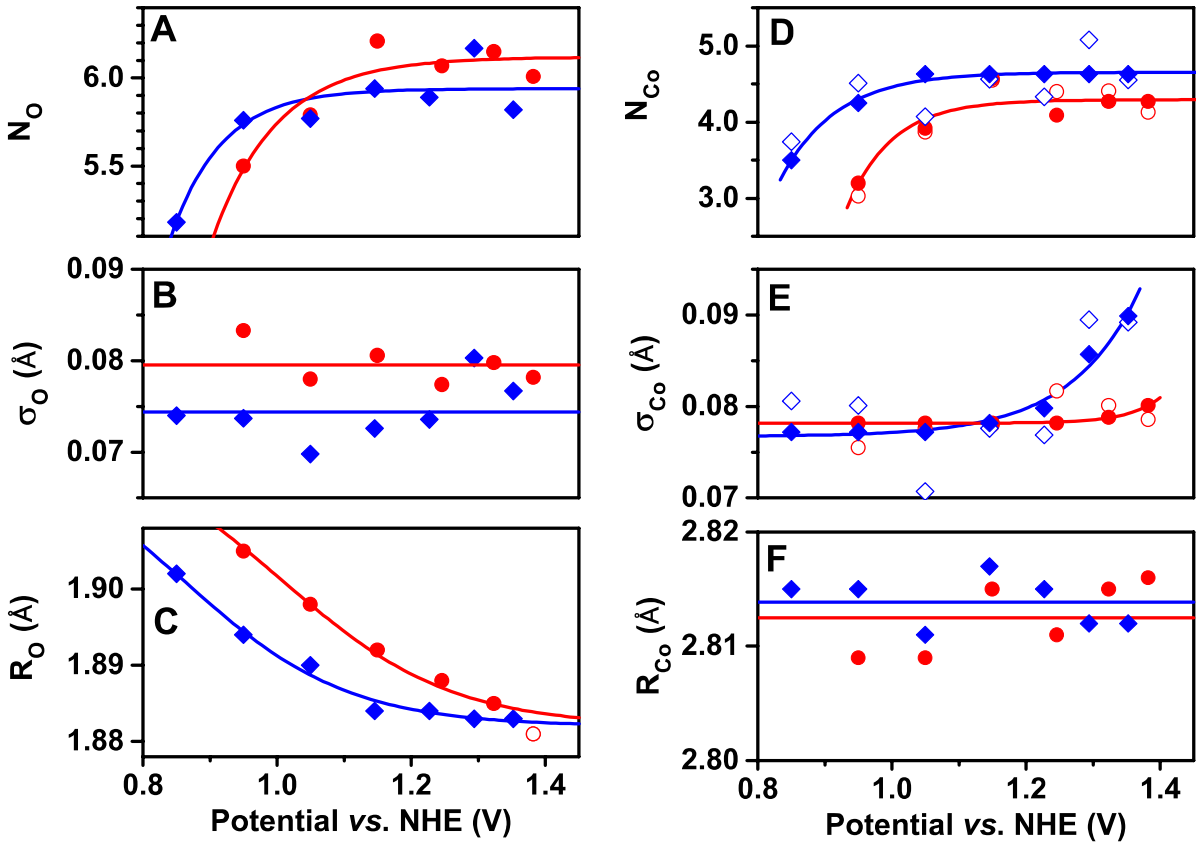

Figure S9. Results for simulation (curve-fitting) of the EXAFS for the Co—O interactions of the first Co coordination sphere (A, B, C) and the Co—Co interactions assignable to di-μ-oxo bridged Co ions (D, E, F). The shown measurements were obtained by the *in-situ* method at pH 7 (red circles) and at pH 9 (blue diamonds). The simulated parameters were the number of scattering atoms, N_i, of element i at distance R_i from the absorbing cobalt atom and the Debye-Waller parameter, σ_i, that is related to the width of the distance distribution function centered at R_i. Filled symbols in panels D and E indicate alternative simulations for which either σ or N was fixed. Lines were added to guide the eye.

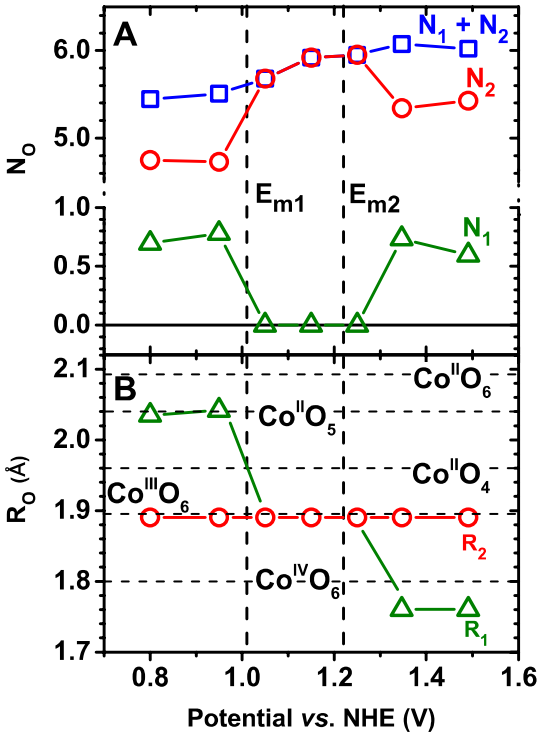

Figure S10 Refined EXAFS simulation for the Co—O vectors of the first Co coordination sphere (freeze-quench data, pH 7). The quality of the simulation improved if a second Co species (Co^{II} or Co^{IV}; triangles) was added to Co^{III} (circles); their sum is shown as squares. The Debye-Waller factor of all species was fixed at 0.045 Å, in order to avoid undesirable parameter correlations and the Co^{III}—O bond length was fixed at 1.89 Å. The coordination numbers, N_i, and distance, R_i, varied freely. However, we enforced a common Co^{IV}—O bond length. Horizontal dashed lines in (B) indicate typical literature values of Co—O bond lengths.[15,16] The combined coordination number of both species is shown for comparison with the simulations in Fig. 10. The two dashed vertical lines indicate the position of the midpoint potentials E_{m1} and E_{m2}.

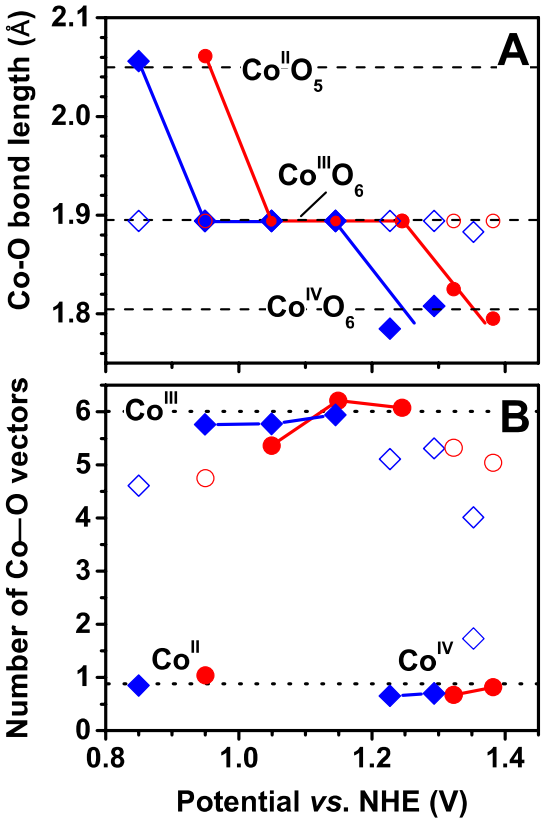

Figure S11. Refined simulation of the Co *K*-edge EXAFS for Co—O vectors of the first Co coordination sphere. The EXAFS spectra were obtained by the *in-situ* method at pH 7 (red circles) and at pH 9 (blue diamonds). The simulations were performed for either one cobalt species or two cobalt species. In the latter case, open symbols indicate Co^{III} contributions, whereas closed symbols indicate contribution assigned either to Co^{II}, at low potentials, or to Co^{IV}, at high potentials. The Debye-Waller parameter of all species was fixed at 0.045 Å, in order to avoid undesirable parameter correlations, and the Co^{III}—O bond length was fixed at 1.89 Å. The coordination numbers, N_i, and distance, R_i, varied freely. The dashed horizontal lines in (B) indicate typical literature values for Co—O bond lengths.[15,16]

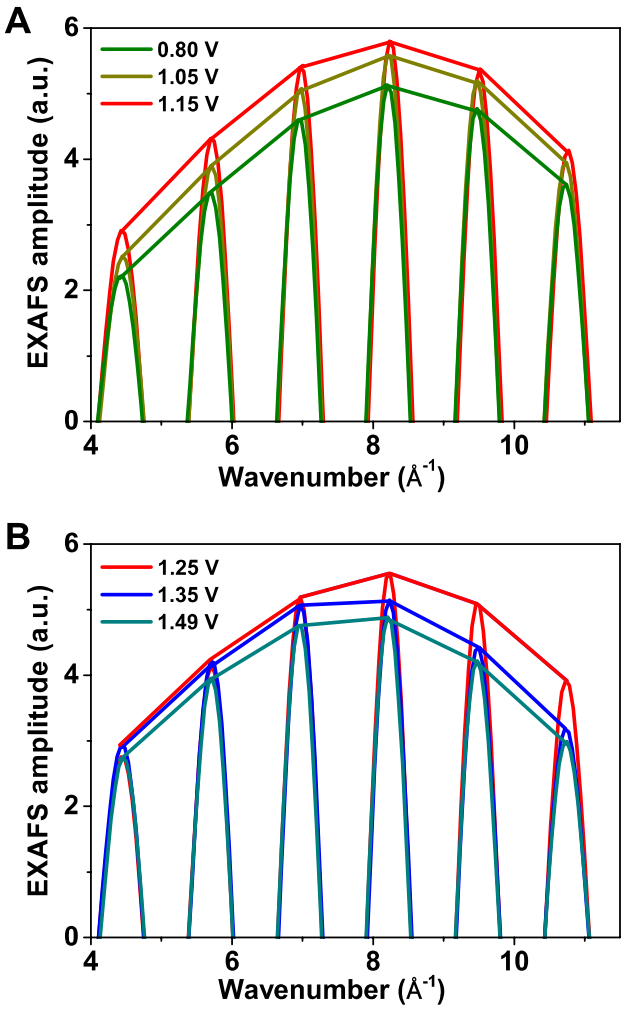

Figure S12. EXAFS oscillations corresponding to the Co—Co peak of the data of Fig. S8A. The indicated voltages give the electrode potential *vs.* NHE. The shown oscillations were obtained by means of Fourier-isolation of data ranging from 2.1 $Å^{-1}$ to 2.9 $Å^{-1}$ (on the reduced distance scale of Fig. S8A); for clarity, only the positive amplitudes of the EXAFS oscillations are shown. Panel A corroborates the simulation result that the coordination number increases with the potential up to 1.15 V (increased amplitude at all wavenumbers), and panel B shows that for high potentials, the peak reduction observed in the Fourier transform is due to an increase of the Debye-Waller parameter (visible as amplitude reduction most pronounced at wavenumbers greater 8 $Å^{-1}$).

REFERENCES

(1) Schaefers, F.; Mertin, M.; Gorgoi, M. *Rev. Sci. Instrum.* **2007**, *78*, 123102.

(2) Ankudinov, A. L.; Ravel, B.; Rehr, J. J.; Conradson, S. D. *Phys. Rev. B: Condens. Matter* **1998**, *58*, 7565.

(3) Rehr, J. J.; Kas, J. J.; Prange, M. P.; Sorini, A. P.; Takimoto, Y.; Vila, F. *Comptes Rendus Physique* **2009**, *10*, 548.

(4) Stern, E. A. B., B.; Heald, S.M. In *EXAFS Spectroscopy, Techniques and Applications*; Teo, B. K. J., D.C., Ed.; Plenum Press: New York and London, 1981.

(5) Rehr, J. J.; Albers, R. C. *Rev. Mod. Phys.* **2000**, *72*, 621.

(6) Risch, M.; Khare, V.; Zaharieva, I.; Gerencser, L.; Chernev, P.; Dau, H. *J. Am. Chem. Soc.* **2009**, *131*, 6936.

(7) Dau, H.; Limberg, C.; Reier, T.; Risch, M.; Roggan, S.; Strasser, P. *ChemCatChem* **2010**, *2*, 724.

(8) Dau, H.; Liebisch, P.; Haumann, M. *Anal. Bioanal. Chem.* **2003**, *376*, 562.

(9) Hoogvliet, J. C.; Dijksma, M.; Kamp, B.; van Bennekom, W. P. *Anal. Chem.* **2000**, *72*, 2016.

(10) Huheey, J. E.; Keiter, E. A.; Keiter, R. l. *Inorganic chemistry: Principles of structure and reactivity*; Addison Wesley, 1993.

(11) Liebisch, P.; Haumann, M.; Dau, H. *Phys. Scr.* **2005**, *T115*, 859.

(12) Yamamoto, T. *X-Ray Spectrom.* **2008**, *37*, 572.

(13) Mattioli, G.; Risch, M.; Bonapasta, M. A.; Dau, H.; Guidoni, L. *Phys. Chem. Chem. Phys.* **2011**, *13*, 15437.

(14) Risch, M.; Ringleb, F.; Khare, V.; Chernev, P.; Zaharieva, I.; Dau, H. *J. Physics: Conf. Series* **2009**, *190*, 012167.

(15) Wood, R. M.; Palenik, G. J. *Inorg. Chem.* **1998**, *37*, 4149.

(16) Lalena, J. N.; Cleary, D. A. *Principles of inorganic materials design*; John Wiley and Sons, 2010.